

QCD CORRECTIONS TO HEAVY QUARK PAIR PRODUCTION IN POLARIZED $\gamma\gamma$ COLLISIONS AND THE INTERMEDIATE MASS HIGGS SIGNAL

G. Jikia

*Institute for High Energy Physics
Protvino, Moscow region, 142284, Russia*

A. Tkabladze

*Bogoliubov Laboratory of Theoretical Physics,
JINR, Dubna, Moscow Region, 141980, Russia*

Abstract

Perturbative QCD one-loop corrections to the cross sections of the $b\bar{b}(c\bar{c})$ quark pair production in polarized photon-photon collisions, as well as cross sections of the radiative processes $\gamma\gamma \rightarrow b\bar{b}g$, $c\bar{c}g$ leading to two- and three-jet final states are calculated. It is shown that the signal from the intermediate mass Higgs boson is observable and precise measurements of the Higgs boson two-photon width are possible at a photon-photon collider, although the statistical significance is substantially reduced with respect to the tree level calculations. We demonstrate that virtual corrections are of the same order or larger than the Born contribution in the $J_z = 0$ channel at high energy for small values of the cutoff y_{cut} , separating two-jet from three-jet topologies. The nature of these large corrections is elucidated. For $b\bar{b}$ pair production at $\sqrt{s_{\gamma\gamma}} \sim 100$ GeV and for small values of $y_{cut} \leq 0.04$ the higher order resummation of double logarithmic terms $\mathcal{O}(\alpha_s m_b^2/s \ln^2(s/m_b^2))$ is needed.

1 Introduction

Higgs boson search and study of the electroweak symmetry breaking mechanism will be major goals for the next generation of supercolliders[1, 2]. Despite excellent successes of the standard model (SM) in describing of experimental data of electroweak interactions of gauge bosons and fermions, no evidence, even indirect, for the Higgs boson sector of the theory has been given yet. Much has been written on the search for the SM Higgs boson at Hadron Supercolliders (see e.g. ref [2] for recent reviews and further references).

A Higgs particle with mass above $2m_W$ ($2m_Z$) can be produced and detected in its W^+W^- or ZZ decay mode at high-energy hadron colliders because the continuum of massive vector boson pair production is significantly small. It is generally believed that a Higgs boson of mass up to 1 TeV (and larger than $2m_W$) can be discovered at LHC if the design luminosity is achieved.

The most difficult range of the Higgs boson mass to probe at Hadron Colliders is the so-called intermediate mass region, beyond the reach of LEP-200 and below the mass, where the Higgs has a decay channel into two massive gauge bosons (WW, ZZ), $90 \text{ GeV} < m_H < 2m_W(m_Z)$. Discovery of the intermediate mass Higgs boson at Hadron Colliders is possible through the rare decays with light leptons and photons in final states, $H \rightarrow ZZ^* \rightarrow l^+l^-l^+l^-$, $H \rightarrow \gamma\gamma$ [3], or associated WH production $WH \rightarrow l\nu\gamma\gamma$ [4]. The combination of these modes provides a possibility of covering the whole intermediate mass region at LHC only in the case when the $\gamma\gamma$ resolution is adequate to resolve the $H \rightarrow \gamma\gamma$ signal and high luminosity ($L = 10^5 \text{ pb}^{-1}$) is achieved [3, 4]. For the SM Higgs boson of intermediate mass primary decay mode is $H \rightarrow b\bar{b}$ but, unfortunately, detection of Higgs through heavy quark pairs is impossible due to large QCD backgrounds [1].

The collision of high energy, high intensity photon beams at the Photon Linear Collider (PLC), obtained via Compton backscattering of laser beams off linac electron beams, provides another opportunity to search for an intermediate-mass Higgs boson through the resonant production [5, 6, 7, 8, 9, 12]

$$\gamma\gamma \rightarrow H \rightarrow b\bar{b}. \quad (1)$$

Based on the e^+e^- linear collider PLC will have almost the same energy and luminosity, i.e. c.m. energy of 100–500 GeV and luminosity of the order of $10^{33} \text{ cm}^{-2}\text{s}^{-1}$ [10]. Polarizing the linac electrons and laser photons provides polarized backscattered photons as well as photon energy distribution needed. Colliding like-handed electrons and photons results in a flat distribution of backscattered photons and colliding oppositely handed electrons and laser photons gives a peaked distribution of backscattered photons with energy just below the e^+e^- -collider energy.

Extracting the intermediate mass Higgs signal in photon-photon collisions is a hard task since a large number of $b\bar{b}/c\bar{c}$ background events must be rejected [5, 6, 11, 12]. The crucial assumption is that these large backgrounds can actively be suppressed by exploiting the polarization dependence of the cross sections. Far above the threshold, the $\gamma\gamma \rightarrow q\bar{q}$ cross section is dominated by initial photons in the $J_z = \pm 2$ helicity state. Taking into account that the Higgs signal comes from the $J_z = 0$ channel, polarized collisions can be used to enhance the signal simultaneously suppressing the background [5, 6] (see also a detailed discussion in [7, 12]). The search for intermediate-mass Higgs requires not only luminosity distribution dominating at $J_z = 0$. Another important requirement to $\gamma\gamma$ -luminosity is that it must cover the entire intermediate mass region. Utilizing the broad photon-photon luminosity at fixed linac energy of 125 GeV provides high $\gamma\gamma$ -luminosity and high photon polarization

over the whole region of interest [6].

To study the properties of the Higgs boson of known mass, the peaked photon-photon luminosity spectrum is more convenient, it could be obtained by choosing the collider energy so that the peak of the luminosity spectrum sits at the Higgs boson mass. The Higgs boson production in such collisions would provide an accurate measurement of the $H \rightarrow \gamma\gamma$ coupling. This coupling is induced at the one-loop level and receives contributions from all virtual charged particles whose masses derive from the Higgs mechanism. The measurement of the $H \rightarrow \gamma\gamma$ coupling would give fundamental information about the particle spectrum and mass generation mechanism of the theory. In addition, a new interesting method has been proposed [13, 14] to measure the parity of the Higgs states in linearly polarized photon-photon collisions. It provides an opportunity to investigate nontrivial assignments of the quantum numbers for Higgs particles in extended models such as supersymmetric theories which include both scalar 0^{++} and pseudoscalar 0^{-+} states [15].

But the question remains how QCD radiative corrections influence these conclusions. Though it is known that far above the threshold the magnitude of these corrections is moderate for unpolarized collisions [16, 17], one can expect that their effects will be especially large for the $q\bar{q}$ production in the $J_z = 0$ helicity state, where the tree level contribution is suppressed by the factor of m_q^2/s . We presented our first results on the one-loop QCD corrections to the $b\bar{b}/c\bar{c}$ quark pair production in polarized photon-photon collisions in [18]. The lowest order cross section, one-loop virtual corrections and gluon emission contributions were shown to be of the same order of magnitude for the $b\bar{b}$ quark production at $\sqrt{s_{\gamma\gamma}} \sim 100$ GeV in the $J_z = 0$ channel, while QCD corrections were found to be quite small for $J_z = \pm 2$. The cross section of two-jet final states in $b\bar{b}(g)$ production for $J_z = 0$ even happened to be negative for small values of y_{cut} (which were used *e.g.* in [7], where only radiative processes of $b\bar{b}g$ production were taken into account for $m_b = 0$). Here we present complete analytical results for the one loop QCD corrections to the polarized cross sections and to the matrix element of the process $\gamma\gamma \rightarrow b\bar{b}(c\bar{c})$ retaining the full dependence on the quark mass. We also carefully analyze the nature of the peculiarities of the corrections for $b\bar{b}$ production at high energies in the $J_z = 0$ channel. We exploit a tensor reduction algorithm [21] to express the cross sections and amplitudes in terms of the set of basic scalar loop integrals. This leads to very compact expressions for one loop contributions for polarized cross sections.

Recently, the next-to-leading order corrections to the heavy quark pair production cross sections in polarized photon-photon collisions have been also presented in ref. [19], where dimensional reduction have been used to regularize both ultraviolet and infrared singularities. Authors of ref. [19] considered the effects of the QCD corrections on the background events for the Higgs signal from direct $b\bar{b}(g)$ production only for Higgs boson production at the photon machine obtained from a 500 GeV e^+e^- linear collider. However, it has been explicitly shown in refs. [11, 12], where all backgrounds from two-jet productions were included: direct, so-called resolved and twice-resolved

etc., that the major contribution to the background at 500 GeV is the 1-resolved coming from the gluonic content of the photon, not the direct. Another backgrounds occur in processes where c -quarks are produced instead of b -quarks. Since charm production is much larger than b production, due to the c -quark's stronger coupling to the photon, it represents an important background even with good b -tagging and a low probability that c -quark is misidentified as a b . The charm background is also not considered in [19].

In present paper we study the effects of QCD corrections on the ability of PLC to discover an intermediate mass Higgs boson for the case of a photon collider operating at around the Higgs resonance based on the e^+e^- collider with energy $\sqrt{s} = 250$ GeV. The resolved photon backgrounds are much less significant at 250 GeV due to a steeply falling gluon spectrum. We use dimensional regularization to regulate ultraviolet divergencies and introduce a small gluon mass λ to regulate infrared divergencies. Analytical results are given in Sections 2–4 and Appendices A, B. In section 5 numerical results are given. It is shown that taking account of the QCD corrections reduces the signal-to-background ratio but the intermediate mass Higgs boson signal is still expected with statistical significance of about 5σ . The influence of QCD corrections on the precise measurements of the Higgs two-photon width using the peaked $\gamma\gamma$ luminosity is also considered.

2 Born Cross Sections

At the tree level the cross sections of the quark-antiquark pair production in the photon-photon fusion reaction

$$\gamma(p_1)\gamma(p_2) \rightarrow b(p_3)\bar{b}(p_4) \quad (1)$$

for various helicity states of the colliding photons have the form

$$\frac{d\sigma^{Born}(J_z = 0)}{dt} = \frac{12\pi\alpha^2 Q_b^4 m_b^2 s^2 (s - 2m_b^2)}{s^2 t_1^2 u_1^2}, \quad (2)$$

and

$$\frac{d\sigma^{Born}(J_z = \pm 2)}{dt} = \frac{12\pi\alpha^2 Q_b^4 (t_1 u_1 - m_b^2 s)(u_1^2 + t_1^2 + 2m_b^2 s)}{s^2 t_1^2 u_1^2}. \quad (3)$$

We have introduced the following notation: p_1, p_2 are the photon momenta, p_3 and p_4 are quark and anti-quark momenta. $s = (p_1 + p_2)^2$, $t = (p_1 - p_3)^2$, $u = (p_1 - p_4)^2$, $t_1 = t - m_b^2$, $u_1 = u - m_b^2$.

The $J_z = 0$ cross section is suppressed by m_b^2/s factor at high energies outside the very forward (backward) region. However, the total cross section integrated over the full phase space is not suppressed, so in the high energy limit the $J_z = 0$ cross section tends to a delta-function, peaking in the forward (backward) direction.

3 QCD One-Loop Corrections to the Matrix Element

Complete set of the diagrams describing α_s -corrections for the process $\gamma\gamma \rightarrow b\bar{b}$ is shown in Fig. 1. This set contains genuine one-loop diagrams and tree level diagrams involving counterterms.

The full one-loop matrix element (with the corresponding counterterms) can be written as follows

$$T^{(1)}(\gamma\gamma \rightarrow b\bar{b}) = e^2 g^2 a_i(s, t, u) \bar{u}(p_4) \hat{O}_i v(p_3) + (t \leftrightarrow u, p_3 \leftrightarrow p_4), \quad (1)$$

where the set of the operators \hat{O}_i is given by

$$\begin{aligned} \hat{O}_1 &= (e_1 e_2), & \hat{O}_6 &= \hat{p}_1 (e_1 e_2), \\ \hat{O}_2 &= (e_1 p_3)(e_2 p_3), & \hat{O}_7 &= \hat{p}_1 (e_1 p_3)(e_2 p_3), \\ \hat{O}_3 &= \hat{e}_1 \hat{p}_1 (e_2 p_3) - \hat{e}_2 \hat{p}_1 (e_1 p_3), & \hat{O}_8 &= \hat{e}_1 \hat{e}_2, \\ \hat{O}_4 &= \hat{e}_1 (e_2 p_3), & \hat{O}_9 &= \hat{e}_1 \hat{e}_2 \hat{p}_1. \\ \hat{O}_5 &= \hat{e}_2 (e_1 p_3), \end{aligned}$$

Here e_1, e_2 are the photon polarization vectors. To simplify the final expressions, photon polarization vectors are chosen so as to fulfil the relations $(e_2 p_1) = 0$ and $(e_1 p_2) = 0$.

The coefficients $a_i(s, t, u)$ expressed through the scalar one-loop integrals defined in the Appendix A are given in the Appendix B. The algebraic calculation of one-loop diagrams was carried out by using the symbolic manipulation program FORM [22]. The finite parts of the counterterms are fixed by the standard conditions of the on-mass shell renormalization procedure. The sum of the diagrams is UV-finite and gauge invariant. To avoid infrared singularities, we have introduced an infinitesimal mass of the gluon λ .

4 QCD One-Loop Corrections to Polarized Cross Sections

The cross sections to order $\alpha^2 \alpha_s$ are determined by the interference between one-loop and tree level contributions given in the previous sections. For the different helicities of two photons ($J_z = 0$ and $J_z = \pm 2$) they have the form

$$\begin{aligned} \frac{d\sigma(J_z = 0)}{dt} &= \frac{\alpha^2 \alpha_s Q_b^4}{s^2} \\ &\frac{16m_b^2 s}{t_1 u_1} \left\{ (t+u)^2 D(s, t) + 2m_b^2 C(s) + \frac{2m_b^2 s}{t_1} C_1(t) \right\} \end{aligned}$$

$$\begin{aligned}
& - \frac{3tu + m_b^2 u + 3t^2 - m_b^2 t - 2m_b^4}{t_1^2} B(t) - \frac{2(s^2 - t_1 u_1) + s s_4}{2t_1 u_1} \\
& + \frac{s(u+t)}{2t_1 u_1} \ln\left(\frac{\lambda^2}{m_b^2}\right) + (t \leftrightarrow u) \Big\}, \tag{1}
\end{aligned}$$

$$\begin{aligned}
\frac{d\sigma(J_z = \pm 2)}{dt} &= \frac{2 \alpha^2 \alpha_s Q_b^4}{s^2} \\
& \Big\{ \left(-\frac{8m_b^2 s s_4}{t_1 u_1} + \frac{8s(st_1 + 8m_b^4)}{u_1} - 4(su_1 - 2m_b^2 s - 8m_b^4) \right) D(s, t) \\
& + \frac{2s(3s^2 - 2t_1 u_1 - 16m_b^4)}{t_1 u_1} C(s) + \frac{2s_4(s^2 + 2t_1 u_1 + 2m_b^2 s)}{t_1 u_1} C_1(s) \\
& + \frac{8(2m_b^2(u-t) + t_1^2 + s^2 - 8m_b^2)}{u_1} C_1(t) \\
& - \frac{4Y}{t_1 u_1} \left(\frac{t_1 t_2 u_1 - 2s(t^2 + m_b^4) - 8m_b^2 t^2}{tt_1^2} B(t) - \frac{2s}{s_4} B(s) \right. \\
& + \left. \frac{u_1^2 + t_1^2 + 2m_b^2 s}{t_1 u_1} \ln\left(\frac{\lambda^2}{m_b^2}\right) \right) \\
& - \frac{32m_b^2}{su_1} (Y + u_1 u_2) - \frac{4}{u_1} \left(\frac{t_1(3u - m_b^2)}{u_1} - \frac{2m_b^4}{t} \right) + \frac{4m_b^2}{u} \\
& + (t \leftrightarrow u) \Big\}, \tag{2}
\end{aligned}$$

where $s_4 = s - 4m_b^2$, $t_1 = t - m_b^2$, $u_1 = u - m_b^2$, $t_2 = t + m_b^2$, $u_2 = u + m_b^2$ and $Y = ut - m_b^4$.

The explicit forms of the scalar functions D , C and B are given in the Appendix A. The IR divergencies are canceled out if one takes into account the contribution of the soft gluon emission

$$\frac{d\sigma^{soft}}{dt} = \frac{d\sigma^{tree}}{dt} R^{soft}, \tag{3}$$

where

$$\begin{aligned}
R^{soft} &= \frac{8\alpha_s}{3\pi} \Big\{ \left(-1 + \frac{1}{\beta} \left(1 - \frac{2m_b^2}{s} \right) \ln\left(\frac{1+\beta}{1-\beta}\right) \right) \ln\left(\frac{2k_c}{\lambda}\right) + \\
& \frac{1}{2\beta} \ln\left(\frac{1+\beta}{1-\beta}\right) + \frac{1}{2\beta} \left(1 - \frac{2m_b^2}{s} \right) \left[Sp\left(\frac{-2\beta}{1-\beta}\right) - Sp\left(\frac{2\beta}{1+\beta}\right) \right] \Big\} \tag{4}
\end{aligned}$$

and k_c is the soft gluon energy cut and $\beta = \sqrt{1 - 4m_b^2/s}$.

The cross section of hard gluon emission is evaluated numerically. The matrix element squared is calculated by using FORM and also by means of COMPHEP

system [23]. The results are quite lengthy to be presented here and coincide with each other numerically. The integration over three-particle phase space is done by using Monte-Carlo integration routine VEGAS [27]. Special care is taken to handle sharp peaks of the cross section arising when gluon is soft and when gluon is emitted along the quark or anti-quark momentum and corresponding to the infrared and collinear singularities. In order that VEGAS algorithm converged fast enough all the singularities must be running along the axes of the integration variables (see detailed discussion in [28]). We take gluon energy, the denominator of the quark propagator and quark and anti-quark production angles as integration variables, so that the infrared and collinear as well as t -channel singularities all run along some axis.

The total cross section for $b\bar{b}$ production can be cast into the form [16]

$$\sigma_{\lambda_1\lambda_2}^{\gamma\gamma\rightarrow b\bar{b}(g)} = \frac{\alpha^2 Q_b^4 N_c}{s} \left[f_{\lambda_1\lambda_2}^{(0)} + \frac{4\alpha_s}{3\pi} f_{\lambda_1\lambda_2}^{(1)} \right], \quad (5)$$

where $f_{++,-}^{(0,1)}$ depend on the dimensionless variable $s/(4m_q^2)$ only. In Table 1 the values of the functions $f_{++,-}^{(0,1)}$ are presented for various helicity states of initial photons and for the case of unpolarized photon collisions versus $s/(4m_b^2)$. Both $f_{++}^{(0)}$ and $f_{++}^{(1)}$ are not suppressed at high energies, because no angular cut is imposed in Table 1 (*cf.* Section 2). While $f_{+-}^{(1)}$ is always positive and monotonically rising, $f_{++}^{(1)}$ has a minimum near to $s/(4m_b^2) \sim 9$, where it is negative. The value of $f_{++}^{(1)}$ at threshold is not zero due to a familiar Sommerfelds rescattering correction. The values of one-loop correction function $f_{unpol}^{(1)}$ obtained for unpolarized photon collisions

$$f_{unpol}^{(0,1)} = \frac{1}{2} (f_{++}^{(0,1)} + f_{+-}^{(0,1)}) \quad (6)$$

agree with the results of papers [16, 17] to the accuracy better than 0.3%.

The total cross sections calculated up to the order $\alpha^2\alpha_s$ are given by the sum of the tree-level contribution (Section 2), the interference term between the one-loop and tree-level contributions, and the tree level contribution from the quark pair production accompanied by the gluon emission $\gamma\gamma \rightarrow q\bar{q}g$. The first two contributions lead to two parton final states converting mainly into two jets, while the third one leads to the three parton production converting both into two- and three-jet final states. The reason is that three parton final states with collinear and/or soft gluon will appear experimentally as two jets. Moreover, only the sum of cross sections of $q\bar{q}$ and $q\bar{q}g$ production with the soft or collinear gluon is free from infrared divergencies and has no mass singularities in the limit $m_q \rightarrow 0$. So, as usual, we consider the three parton state to represent the two-jet final state if the invariant mass of two partons is sufficiently small

$$s_{ij} < y_{cut}s_{\gamma\gamma}, \quad (7)$$

where $s_{ij} = (p_i + p_j)^2$ is the invariant mass squared of two partons i and j and $\sqrt{s_{\gamma\gamma}}$ is the total c.m.s. energy of two colliding photons.

$\frac{s}{4m_b^2}$	$f_{++}^{(0)}$	$f_{+-}^{(0)}$	$f_{unpol}^{(0)}$	$f_{++}^{(1)}$	$f_{+-}^{(1)}$	$f_{unpol}^{(1)}$
1	0	0	0	124	0	62.0
4	26.3	27.2	26.7	7.05	82.2	44.6
9	27.0	44.5	35.8	-2.95	129	62.8
16	26.7	57.4	42.1	29.1	169	99.2
25	26.4	67.7	47.1	72.6	208	140
100	25.6	101	63.3	292	388	340
400	25.3	135	80.3	618	724	671
2500	25.2	181	103	1200	1530	1370

Table 1: Functions $f^{(0,1)}$ for various values of $\frac{s}{4m_b^2}$ for polarized and unpolarized incoming photons.

Fig. 2 shows the total (*i.e.* two-jet plus three-jet) and two-jet ($y_{cut} = 0.08$) cross sections for the $b\bar{b}/c\bar{c}$ pair production in polarized monochromatic $\gamma\gamma$ collisions. Throughout we use a two-loop expression for $\alpha_s(Q^2)$ with $\Lambda = 200$ MeV, $Q^2 = s$ and $N_F = 5$ as the number of flavors. We take $m_b = 5$ GeV and $m_c = 1.5$ GeV. The angular cut $|\cos\theta| < 0.7$ means a cut on the scattering angles of both quark and anti-quark. This choice is different from that used in [19], where only the quark scattering angle is restricted.

While the QCD corrections for the $J_z = \pm 2$ photon helicities are quite small, those for $J_z = 0$ enhance $c\bar{c}$ production by an order of magnitude or even larger. For the $b\bar{b}$ production the situation is more complicated: the corrected total cross section is smaller than the tree level $\gamma\gamma \rightarrow b\bar{b}$ cross section for $\sqrt{s_{\gamma\gamma}} < 85$ GeV and larger for larger energies. The effect is more pronounced for the two-jet production.

For small values of $y_{cut} < 0.04$ the two-jet differential cross section in $J_z = 0$ channel is even negative in some regions of the phase space. Fig. 3 gives the differential cross sections for the $b\bar{b}$ pair production versus the scattering angle at $\sqrt{s_{\gamma\gamma}} = 100$ GeV for various helicity states of initial photons and various cuts. As it is shown in Fig. 3a, for $J_z = 0$ and $y_{cut} = 0.04$ differential cross section becomes negative in the central region of the scattering angles. This means that for the $b\bar{b}$ production at $\sqrt{s_{\gamma\gamma}} \sim 100$ GeV all the three contributions (Born, virtual and real gluon emission) are of the same order of magnitude and perturbation expansion is not valid for too small values of $y_{cut} \leq 0.04$. This is unlike the case of the $c\bar{c}$ production, where the real gluon emission contribution still dominates for $y_{cut} = 0.04$.

To elucidate the breakdown of the perturbative expansion for $b\bar{b}$ production in the $J_z = 0$ channel at high energies we present the sum of virtual and soft gluon emission contributions in the limit $s, -t, -u \gg m_b^2$ under the double logarithmic

approximation

$$\begin{aligned}
\frac{d\sigma^{soft+virt}(J_z = 0)}{d\cos\theta} = & -\frac{4\alpha_s\alpha^2 Q_b^4 m_b^2}{s} \left\{ -2\left(\frac{s}{t} + \frac{s}{u}\right) \ln^2\left(\frac{s}{m_b^2}\right) \right. \\
& + \frac{s^2}{t^2} \ln\left(\frac{s}{m_b^2}\right) \left(\ln\left(\frac{s}{m_b^2}\right) + 4\ln\left(-\frac{t}{m_b^2}\right) \right) \\
& + \frac{s^2}{u^2} \ln\left(\frac{s}{m_b^2}\right) \left(\ln\left(\frac{s}{m_b^2}\right) + 4\ln\left(-\frac{u}{m_b^2}\right) \right) \\
& + 4\frac{s^2}{tu} \ln\left(\frac{s}{m_b^2}\right) \left(\ln\left(-\frac{t}{m_b^2}\right) + \ln\left(-\frac{u}{m_b^2}\right) \right) \\
& \left. - 2\left(\frac{s^2}{t^2} + \frac{s^2}{u^2} - 2\frac{s}{t} - 2\frac{s}{u}\right) \ln\left(\frac{s}{m_b^2}\right) \ln\left(\frac{4k_c^2}{m_b^2}\right) \right\}. \tag{8}
\end{aligned}$$

It is this large negative double logarithmic contribution which makes two-jet cross section negative. Normally, (and this is the case for $J_z = 2$ channel) $\ln^2(s/m^2)$ terms are cancelled out. This is a consequence of the Kinoshita-Lee-Nauenberg theorem [29] stating that cross sections integrated over all degenerate in energy final states are free from mass singularities. However, this theorem is trivially fulfilled for $J_z = 0$ channel, as Born cross section, virtual correction and soft gluon emission are all equal to zero for $m_b = 0$. The cross section of the hard gluon emission $\sigma(\gamma\gamma \rightarrow b\bar{b}g)$ in principle is not suppressed in the $J_z = 0$ channel in the limit $m_b = 0$. But selecting only two-jet topologies for $y_{cut} \ll 1$ we suppress also the cross section of the hard gluon emission. It is worth mentioning, that cross section of $b\bar{b}g$ production also contains subleading double logarithmic terms of the order $\mathcal{O}(\alpha^2\alpha_s m_b^2/s \ln(s/m_b^2) \ln(s/k_c^2))$, but they do not completely cancel the double logarithmic terms (8). Consider two final state jets to lie in the central region of the detector with $|\cos\theta| < \Delta z \ll 1$. Then $J_z = 0$ cross sections are given by

$$\begin{aligned}
\Delta\sigma^{Born} &= \frac{192\pi\alpha^2 Q_b^4 m_b^2}{s} \frac{\Delta z}{s} \\
\Delta\sigma^{soft+virt} &= -\frac{384\alpha_s\alpha^2 Q_b^4 m_b^2}{s} \frac{1}{s} \ln^2\left(\frac{s}{m_b^2}\right) \Delta z \\
\Delta\sigma^{hard} &= \frac{128\alpha_s\alpha^2 Q_b^4}{s} \left(2y_{cut} \ln\frac{1}{2y_{cut}} - y_{cut} \right) \Delta z. \tag{9}
\end{aligned}$$

The last cross section was calculated in ref. [7]. We take $k_c = \sqrt{s}/2$ in (8) to take into account a partial cancellation of double logarithmic terms between contribution (8) and the hard gluon emission contribution, calculated for finite value of $m_b \neq 0$. The ratio of $\sigma^{soft+virt}/\sigma^{Born}$ is equal to $-2\alpha_s/\pi \ln^2(s/m_b^2)$ and at 100 GeV virtual correction is (-2.7) times larger than Born cross section of $b\bar{b}$ pair production! For a y_{cut} of 0.02, as it has been used in [7], virtual correction is also (-2.5) times larger than the cross section of $b\bar{b}g$ production at $\sqrt{s_{\gamma\gamma}} = 100$ GeV. For $c\bar{c}$ production both

virtual correction and Born cross section are an order of magnitude smaller and total cross section is dominated by $c\bar{c}g$ production contribution. Therefore, the approach of [7], where only contributions from the radiative processes $\gamma\gamma \rightarrow c\bar{c}g$, $b\bar{b}g$ have been taken into account in the limit $m_c = m_b = 0$ and stringent value of $y_{cut} = 0.02$ has been used to select two-jet-like events, might be relevant for the $c\bar{c}$ production, but is definitely not applicable for the $b\bar{b}$ production, where higher order resummation of double logarithmic terms is necessary. However, for a loose value of $y_{cut} = 0.08$ and a nonzero value of the b -quark mass the cross section of the radiative process $\gamma\gamma \rightarrow b\bar{b}g$ is large enough for the total cross section to be always positive.

Note also that in the limit $m_b = 0$ one-loop amplitude itself is infrared finite, so we can calculate the $\alpha_s^2\alpha^2$ correction in the zero quark mass limit by just squaring the one-loop amplitude

$$\frac{d\sigma^{(2)}(J_z = 0)}{dt} = \frac{8\alpha_s^2\alpha^2 Q_b^4}{3\pi s^2} \frac{(t-u)^2}{tu}. \quad (10)$$

However, numerically the contribution (10) is negligibly small in the central region.

As one can see from (4.1)–(4.4) the sum of the cross sections of the $q\bar{q}$ production and $q\bar{q}g$ production with the soft gluon does not depend on the gluon mass λ . The cancellation of the dependence on k_c (the soft gluon energy cut) was checked numerically in each case of the two- and three-jet event selection cuts used. For testing the integration method the 2-jet cross section was calculated in two different ways: as a difference between total and 3-jet cross sections and directly using the corresponding cuts for the invariant masses (7). In both cases similar values for the 2-jet cross section were obtained.

For comparison with the results of paper [19] we have calculated the total (2+3 jet), 3-jet and 2-jet cross sections using their cuts. The results are slightly different. We obtained that the total cross sections calculated using our expressions are about 15 – 25% larger than in [19] in both cases of $J_z = 0, \pm 2$. Our 3-jet cross section is about 5% larger for $J_z = \pm 2$ and about 10 – 15% smaller for $J_z = 0$ than those from [19]. But these small differences lead to larger discrepancies for the 2-jet cross sections. For example, at $\sqrt{s} = 40$ GeV for $J_z = 0$ we have got 2-jet cross section which is about 80% larger than that from [19].

5 Higgs Boson Production at Photon Linear Collider

As has been mentioned above, a photon linear collider provides an excellent possibility of searching for the intermediate mass Higgs boson through the resonant $\gamma\gamma \rightarrow H \rightarrow b\bar{b}$ production. In this region of mass, the dominant background to such a process will be the continuum production of heavy quark pairs. As it is discussed previously, at the tree level the quark pair production cross section far above the threshold is

suppressed by a factor of m_q^2/s if two initial photons are in the $J_z = 0$ helicity state from which the Higgs signal comes. So, the use of the $J_z = 0$ dominated photon-photon luminosity distribution reduces the number of background events. Another requirement is that the $\gamma\gamma$ -luminosity must cover the entire intermediate mass region [6]. We make here the same assumptions as in [6], *i.e.*, we choose the broad photon-photon luminosity spectrum resulting from polarized linac electrons and laser light for $\lambda_\gamma \lambda_e > 0$, $\lambda_e = 0.9$, $\lambda_\gamma = 1$, parameter $x = 4.8$ and geometric factor $\rho = 0.6$ [6, 24]. We also assume that the linac beam energy equals 125 GeV and the integrated effective luminosity is 20 fb^{-1} . In Fig. 4, the luminosity distributions for the machine parameters mentioned are plotted.

Our task is to compare the signal and background event rates taking into account the QCD corrections. Fig. 5 shows the event rates of signal and background two-jet final states in photon-photon collisions at tree level (a) and taking into account QCD corrections (b). We ignore here the backgrounds from the $e\gamma \rightarrow eZ \rightarrow ebb$ and $\gamma\gamma \rightarrow f\bar{f}Z$ processes [26], which are essential for $m_H \sim m_Z$. The backgrounds coming from the resolved photon contributions $\gamma g \rightarrow b\bar{b}$, $c\bar{c}$ are also shown. While resolved photon contributions make it very hard to observe the intermediate mass Higgs signal at the 500 GeV linear collider [11] (see, however, recent analysis [12], where conclusion is done that using optimized cuts still it will be possible to extract Higgs signal in the range 110–140 GeV at 500 GeV), these backgrounds are much less significant at 250 GeV due to a steeply falling gluon spectrum (see also [6, 14]). QCD corrections to the Higgs decay into $b\bar{b}$ [25] are also taken into account. We use a cutoff $|\cos\theta| < 0.7$ in the laboratory frame and not in the c.m.s. frame as in [6]. Cut in the laboratory frame gives a slightly better statistical significance of the Higgs signal. Finally, we assumed 5% $c\bar{c}$ -to- $b\bar{b}$ misidentification probability. Thus, the combined background (*i.e.* $b\bar{b} + 0.05c\bar{c}$) is represented by the dotted line and can be compared with the signal denoted by the solid line (Fig. 5b).

Fig. 6 presents the statistical significance of the Higgs boson signal estimated from the tree level and the one-loop calculations including the resolved photon contributions. This plot assumes a 50% $b\bar{b}$ -tagging efficiency for the $b\bar{b}$ final states and the resolution for reconstructing the invariant mass of two-jet events to be Gaussian with $FWHM = 0.1m_H$. From this figure one can conclude that it is advantageous to select two-jet final states and to impose the angular cut in the laboratory frame. The account of the QCD corrections reduces the statistical significance of the Higgs signal almost by a factor of two in comparison with the tree-level result. Nevertheless, the intermediate mass Higgs boson can be observed in $\gamma\gamma$ collisions at least at the level of 5σ in the mass interval from 80 to 160 GeV.

On the other hand, if the intermediate mass Higgs boson is discovered, the PLC gives the best opportunity for measuring the decay width of the Higgs boson into two photons by measuring the resonant production rate of the $b\bar{b}$ pairs, which is proportional to the $H \rightarrow \gamma\gamma$ decay width and the $H \rightarrow b\bar{b}$ decay branching ratio. To measure the two photon width it is more convenient to use the peaked $\gamma\gamma$ luminosity

distribution, which is obtained for the following combination of parameters: $\lambda_e \lambda_\gamma < 0, \rho > 1$. For this configuration, the luminosity distribution is fairly monochromatic ($\sim 10\%$ energy spread) and very highly polarized ($> 95\%$) [6]. Fig. 7 shows the corresponding $\gamma\gamma$ luminosity for both helicity states of two photons. The effective luminosity of 20 fb^{-1} is assumed and parameter ρ is taken to be equal to 3.0 to suppress the low invariant mass tail of the luminosity distribution function.

Considering only $b\bar{b}$ -final states, Fig. 8 gives the expected event rates for the signal and background processes at the tree level and including α_s -corrections. Collider energy is chosen so that the peak of the luminosity spectrum coincides with the mass of the Higgs boson. As in [6], it is assumed that a window in the invariant mass of $\pm 2\sigma$ around the Higgs mass is used for the measurement and the resolution for reconstructing the invariant mass of two-jet events is Gaussian with $\text{FWHM} = 0.1 M_H$. In both cases the angular cut $|\cos \theta| < 0.7$ in the laboratory frame is used, as analogous cut in the c.m.s. frame gives smaller signal to background ratio.

In Fig. 9 the expected statistical errors in the measured two-photon width of the Higgs boson are plotted. For comparison we have presented tree level results with the cut $|\cos \theta| < 0.7$ in both c.m.s. and laboratory frames, and one-loop QCD corrected results in the laboratory frame. Again, 20 fb^{-1} of the integrated effective luminosity and 50% $b\bar{b}$ tagging efficiency with the 5% $c\bar{c}$ contamination are assumed. As one can see from Fig. 9, for the above mentioned parameters the two-photon Higgs boson width can be measured with the statistical error of 6-9% in the wide range of Higgs mass $40 \div 150 \text{ GeV}$. Of course, a more detailed analysis, including full detector simulation, could somewhat modify our estimates of the influence of QCD radiative corrections on the statistical significance of the Higgs signal in photon-photon collisions.

6 Conclusions

In the present paper we consider the influence of the QCD corrections on the background rates for the intermediate mass Higgs boson signal in the process $\gamma\gamma \rightarrow H \rightarrow b\bar{b}$. We have derived compact analytical expressions for the α_s -corrections to the matrix element of the process $\gamma\gamma \rightarrow b\bar{b}(c\bar{c})$ and have calculated QCD corrected heavy quark pair production cross sections in polarized $\gamma\gamma$ collisions. The total cross sections to the order $\alpha^2 \alpha_s$ are calculated retaining the dependance on the quark mass. The cross sections are given by the sum of the tree level cross section, contribution of the interference term between the α_s -correction and the Born amplitude, and the cross sections of quark pair production accompanied by the real gluon emission. The last contribution generates 3-jet events and 2-jet events in the case of radiation of soft or collinear gluon. The contribution of QCD radiative corrections is crucial in the $J_z = 0$ channel for $c\bar{c}$ production enhancing the $c\bar{c}$ event rate by an order of magnitude due to a real gluon emission contribution, which is not suppressed by a

factor of m_q^2/s as is the Born cross section. For $b\bar{b}$ production the situation is more subtle. For small values of $y_{cut} \leq 0.04$, used to separate two- and three-jet final state topologies, virtual correction is negative and of the same order of magnitude as Born and $b\bar{b}g$ production contributions, so that two-jet cross section in the central region is even negative. The origin of this large negative contribution lies in the double logarithmic contribution $\mathcal{O}(\alpha^2 \alpha_s m_b^2/s \ln^2(s/m_b^2))$. Thus, for loose values of $y_{cut} = 0.08$ backgrounds coming from continuum $b\bar{b}(g)$ production are negligible in comparison to ones from $c\bar{c}(g)$ production and one might speculate that the same situation takes place for more stringent values of y_{cut} [7]. However, strictly speaking, to safely estimate $b\bar{b}(g)$ background for small values of y_{cut} the summation of double logarithmic terms is needed.

As a result, we have calculated the backgrounds for the Higgs signal in two-jet events at PLC. It has been shown that the intermediate mass Higgs boson can be observed at the level of 5σ in the mass interval from 40 to 150 GeV for broad spectrum of photon-photon luminosity distribution using suitable cuts. We have also considered the influence of α_s -corrections on the measurement of the two-photon width of the Higgs boson using the peaked $\gamma\gamma$ luminosity. It is shown that for the integrated luminosity of 20 fb^{-1} a measurement of the intermediate mass Higgs boson width $\Gamma(H \rightarrow \gamma\gamma)$ is possible with the statistical error of about 6-9%.

We are grateful to D. Borden and O. Éboli for helpful discussions. This work was supported in part by the International Science Foundation grant NJR000 as well as in part by the joint ISF-RFBR grant NJR300, and in part by the INTAS grant 93-1180.

Appendix A

The scalar four- and three-point functions used are given by the expressions:

$$\begin{aligned}
D(s, t) &= \frac{1}{i\pi^2} \\
&\int \frac{d^4q}{(q^2 - m_b^2)((q + p_1)^2 - m_b^2)((q + p_1 + p_2)^2 - m_b^2)((q - p_4)^2 - \lambda^2)} \\
&= \frac{2}{\beta s(m_b^2 - t)} \left\{ Sp\left(\frac{1}{\beta}\right) - Sp\left(-\frac{1}{\beta}\right) \right. \\
&\quad \left. + \ln\left(-\frac{1-\beta}{1+\beta}\right) \left[\ln\left(1 - \frac{t}{m_b^2}\right) - \frac{1}{2} \ln\left(\frac{\lambda^2}{m_b^2}\right) \right] \right\}; \tag{1}
\end{aligned}$$

where $p_1^2 = 0$, $p_2^2 = 0$, $p_3^2 = m_b^2$ and $p_4^2 = m_b^2$, $\beta = \sqrt{1 - \frac{4m_b^2}{s+i0}}$.

$$\begin{aligned}
C_1(s) &= \frac{1}{i\pi^2} \int \frac{d^4 q}{(q^2 - m_b^2)((q + p_1)^2 - m_b^2)((q + p_1 + p_2)^2 - \lambda^2)} \\
&= \frac{1}{\beta s} \left\{ \ln\left(\frac{\lambda^2}{m_b^2}\right) \ln\left(-\frac{1-\beta}{1+\beta}\right) \right. \\
&\quad \left. + Sp\left(\frac{2}{1+\beta}\right) - Sp\left(\frac{2}{1-\beta}\right) - 2\left[Sp\left(\frac{1}{\beta}\right) - Sp\left(-\frac{1}{\beta}\right)\right] \right\}; \quad (2)
\end{aligned}$$

$p_1 + p_2 + p_3 = 0$, $p_1^2 = s$, $p_2^2 = m_b^2$ and $p_3^2 = m_b^2$.

$$\begin{aligned}
C_1(t) &= \frac{1}{i\pi^2} \int \frac{d^4 q}{(q^2 - m_b^2)((q + p_1)^2 - \lambda^2)((q + p_1 + p_2)^2 - m_b^2)} \\
&= \frac{1}{t - m_b^2} \left\{ \frac{\pi^2}{6} - Sp\left(\frac{t}{m_b^2}\right) \right\}; \quad (3)
\end{aligned}$$

$p_1 + p_2 + p_3 = 0$, $p_1^2 = t$, $p_2^2 = m_b^2$ and $p_3^2 = 0$.

$$\begin{aligned}
C(s) &= \frac{1}{i\pi^2} \int \frac{d^4 q}{(q^2 - m_b^2)((q + p_1)^2 - m_b^2)((q + p_1 + p_2)^2 - m_b^2)} \\
&= \frac{1}{2s} \ln^2\left(-\frac{1-\beta}{1+\beta}\right); \quad (4)
\end{aligned}$$

$p_1 + p_2 + p_3 = 0$, $p_1^2 = 0$, $p_2^2 = 0$ and $p_3^2 = s$.

Only the following combinations of two-point functions are present in the final answer

$$B(s) = \bar{B}(s) - \bar{B}(m_b^2), \quad B(t) = \bar{B}(t) - \bar{B}(m_b^2),$$

where $\bar{B}(s)$ and $\bar{B}(t)$ are the following scalar integrals:

$$\bar{B}(s) = \frac{1}{i\pi^2} \int \frac{d^4 q}{(q^2 - m_b^2)((q + p)^2 - m_b^2)}, \quad (5)$$

$p^2 = s$, and

$$\bar{B}(t) = \frac{1}{i\pi^2} \int \frac{d^4 q}{(q^2 - m_b^2)(q + p)^2}, \quad (6)$$

$p^2 = t$. Thus,

$$B(t) = -\left(1 - \frac{m_b^2}{t}\right) \ln\left(1 - \frac{t}{m_b^2}\right), \quad (7)$$

and

$$B(s) = \beta \ln\left(-\frac{1-\beta}{1+\beta}\right). \quad (8)$$

The functions $C_1(u)$ and $B(u)$ can be obtained by replacing $t \rightarrow u$ in $C_1(t)$ and $B(t)$.

Appendix B

$$\begin{aligned}
a_1(s, t, u) = & \frac{m_b(u-t)}{Y^2} [st_1(7t_1^2 + 2m_b^2t_1 - 4m_b^4) + 2t_1^3(t_1 - 4m_b^2) + 4s^2t^2] D(s, t) \\
& + \left(\frac{4m_b^3}{Y} - \frac{m_bt_1t_2(u-t)}{Y^2} \right) (sC(s) + (u-t)C_1(s) + 2t_1C_1(t)) + \frac{2m_bst}{Y} C(s) \\
& + \frac{4m_btt_1}{Y} C_1(t) + 2m_bt_2 \left(\frac{1}{Y} - \frac{1}{tt_1} \right) B(t) - \frac{2m_bt_1}{Y} B(s) + 2m_b \left(\frac{m_b^2}{tt_1} - \frac{4m_b^2}{Y} \right); \quad (1)
\end{aligned}$$

$$\begin{aligned}
a_2(s, t, u) = & \frac{4m_bs}{Y^3} (m_b^4u + t^3 - 2m_b^4t) [(u-t)(t_1D(s, t) - C_1(s)) - sC(s) \\
& - 2t_1C_1(t)] + \frac{8m_bst_1t_2}{Y^2} (t_1D(s, t) - C_1(s)) + \frac{4m_bs(t(u-t) - t_1t_2)}{t_1Y^2} B(t) \\
& + \frac{4m_b}{Y} \left(\frac{2(m_b^2u + 3m_b^2t_1 - t^2)}{Y} - \frac{2t + s + 6m_b^2}{s_4} \right) B(s) \\
& + \frac{4(Y + t_1u)}{m_bt_1Y} + \frac{4m_b(4t + 5s)}{s_4Y} + \frac{32m_b^3s}{Y^2} - 3; \quad (2)
\end{aligned}$$

$$\begin{aligned}
a_3(s, t, u) = & \frac{2m_b(t_1(t-u) - 3Y)}{Y^2} [tt_1D(s, t) + sC(s) - (t-u)C_1(s) \\
& + 2t_1C_1(t)] + 2m_b \left(6 - \frac{tt_1}{Y} - \frac{m_b^2(u-t)}{Y} \left(1 + \frac{m_b^2s}{Y} \right) \right) D(s, t) \\
& + \frac{4m_bt_1}{Y} C_1(s) + \left(\frac{4m_b}{Y} - \frac{2m_b}{tt_1} \right) B(t) + \frac{4m_b(t-u)}{s_4Y} B(s) \\
& + \frac{16m_bu_2}{s_4Y} + \frac{2m_b}{tt_1}; \quad (3)
\end{aligned}$$

$$\begin{aligned}
a_4(s, t, u) = & \left(\frac{11m_b^2(2tt_1 + m_b^2s) - 7t_1(m_b^4 + t_1s) + 3m_b^4u_1}{Y} - 2u \right. \\
& \left. + \frac{(u-t)t_1^3t_2}{Y^2} \right) D(s, t) + \frac{4m_b^2t_2 - 2t(t+3u)}{Y} C_1(s) + \\
& \left(\frac{2u + 5t}{Y} - \frac{m_b^4s + tt_1^2}{Y^2} \right) [(u-t)(m_b^2D(s, t) + C_1(s)) + sC(s)] + \\
& \left(\frac{4(m_b^2s + 3tt_1)}{Y} + \frac{2(u-t)t_1^3}{Y^2} - \frac{4t}{t_1} \right) C_1(t) - 2 \left(\frac{t_1}{Y} + \frac{m_b^2(3t - m_b^2)}{tt_1^2} \right) B(t) \\
& + \frac{2st_2}{s_4Y} B(s) - \frac{8m_b^2(t-u)}{s_4Y} + \frac{8m_b^2}{t_1^2} - \frac{2}{t}; \quad (4)
\end{aligned}$$

$$\begin{aligned}
a_5(s, t, u) = & \left(\frac{(t^3 t_2 - 6m_b^4 t t_1 + m_b^6 (3s - t_2))(u - t)}{Y^2} \right. \\
& + \frac{m_b^2 t (5u_1 - 6m_b^2) + 3t^2 t_2 + u t_1 t_2}{Y} \Big) D(s, t) \\
& - \frac{s(2m_b^2 t_1^2 - s(t_2^2 + 2m_b^4))}{Y^2} C(s) - \frac{2s(2m_b^2 t^2 (u - t) - (t^2 - 3m_b^4) t_1 t_2)}{t_1 Y^2} C_1(t) + \\
& \left(\frac{2(m_b^2 (u - t) - t t_2)}{Y} - \frac{m_b^4 (4m_b^2 - 3s)(u - t) - t_1 t_2 (t_2^2 - 8m_b^4)}{Y^2} + 1 \right) C_1(s) \\
& + \left(\frac{6t_2}{t_1^2} - \frac{2(t + 3m_b^2)}{Y} \right) B(t) + \frac{2s_4(t - 3m_b^2) - 8m_b^2 t_2}{s_4 Y} B(s) \\
& + \frac{8m_b^2 (2t_2 + 3s_4)}{s_4 Y} - \frac{4t_1 + 6m_b^2}{t_1^2} + \frac{4}{t_1} \ln \left(\frac{\lambda^2}{m_b^2} \right); \tag{5}
\end{aligned}$$

$$\begin{aligned}
a_6(s, t, u) = & -\frac{t_1 t_2 (u - t)}{Y^2} [s_4 t_1 D(s, t) + (u + t) C(s) - s_4 C_1(s) - 2t_2 C_1(t)] \\
& + 2m_b^2 \left(4D(s, t) - \frac{m_b^2 (u - t)^2}{Y^2} C(s) - \left(\frac{2t_2}{Y} - \frac{4}{t_1} \right) C_1(t) \right) \\
& - \left(\frac{2s_4 t_1}{sY} + \frac{8m_b^2}{st_1} - \frac{4}{t_1} - \frac{16m_b^2}{t_1^2} - \frac{2}{t} \right) B(t) + \frac{2t_2}{Y} B(s) \\
& - \frac{8m_b^2 (t - u)}{sY} - \frac{2}{t} + \frac{16m_b^2 (t_1 - 2s)}{st_1^2} + \frac{4}{t_1} \ln \left(\frac{\lambda^2}{m_b^2} \right); \tag{6}
\end{aligned}$$

$$\begin{aligned}
a_7(s, t, u) = & \frac{4(m_b^2 s(u_1 - 4t_1) + t_1^2 (u_1 - s))}{Y^3} [s_4 t_1^2 D(s, t) - st_2 C(s) \\
& - s_4 t_1 C_1(s) - 2t_1 t_2 C_1(t)] + \frac{8m_b^2 s s_4 (m_b^2 s - u_1 t_1)}{Y^3} [t_1 D(s, t) - C_1(s)] \\
& + \frac{4(t_1^3 u_1 - m_b^2 s(3t + m_b^2)^2)}{tt_1 Y^2} (1 - B(t)) - \frac{8stt_2 (2m_b^2 - t_1)}{tt_1 Y^2} B(t) \\
& + \frac{4(2t_1 t_2 - 3Y + 2m_b^2 (u - t))}{Y^2} B(s); \tag{7}
\end{aligned}$$

$$\begin{aligned}
a_8(s, t, u) = & -m_b \left(\frac{s(u - t)m_b^2}{Y} + 3u_1 - t_1 \right) D(s, t) + \frac{m_b s u_1}{Y} C(s) \\
& + \left(4m_b - \frac{m_b s u_2}{Y} \right) C_1(s) + \left(\frac{2m_b^3 s}{Y} - 2m_b \right) C_1(t) + \frac{m_b t_2}{tt_1} B(t) \\
& + \frac{4m_b}{s_4} B(s) - \frac{4m_b}{t_1} + \frac{m_b}{t} - \frac{8m_b}{s_4}; \tag{8}
\end{aligned}$$

$$\begin{aligned}
a_9(s, t, u) = & -\frac{st_2(t_2 - s_4)}{Y}D(s, t) + \frac{s(t_2 - s_4)}{Y}C(s) \\
& + \left(\frac{(m_b^2 - s_4)(u - t) - t_1 t_2}{Y} + 1 \right) C_1(s) + \left(\frac{2t_1(t_2 - s_4)}{Y} - \frac{4m_b^2}{t_1} \right) C_1(t) \\
& - \frac{(3t + m_b^2)t_2}{tt_1^2} B(t) + \frac{16m_b^2}{t_1^2} + \frac{1}{t} - \frac{2}{t_1} \ln \left(\frac{\lambda^2}{m_b^2} \right). \tag{9}
\end{aligned}$$

References

- [1] J.F. Gunion, H.E. Haber, G. Kane and S. Dawson, *The Higgs hunter's guide* (Addison-Wesley Reading, MA, 1990).
- [2] S. Dawson, *Perspectives on Higgs Physics*, ed. G. Kane, World Scientific Publ. (1992), p. 129;
J.F. Gunion, *ibid.*, p. 179;
Z. Kunszt, *ibid.*, p. 156.
- [3] J.F. Gunion, G.L. Kane and J. Wudka, *Nucl. Phys.* **B299** (1988) 231.
- [4] J.F. Gunion, *Phys. Lett.* **B261** (1991) 510;
Z. Kunszt, Z. Trocsanyi and W.J. Stirling, *Phys. Lett.* **B271** (1991) 247.
- [5] J.F. Gunion and H.E. Haber, *Phys. Rev.* **D48** (1993) 5109.
- [6] D.L. Borden, D.A. Bauer, D.O. Caldwell *Phys. Rev.* **D48** (1993) 4018.
- [7] D. L. Borden, V. A. Khoze, W. J. Stirling, and J. Ohnemus, *Phys. Rev.* **D50** (1994) 4499.
- [8] P.M. Zerwas, Proceedings of the VIII Int. Workshop on Photon–Photon Collisions, Shores (Jerusalem Hills) 1988.
- [9] S. Brodsky, in Physics and Experiments with Linear e^+e^- Colliders, Waikoloa, Hawaii, 1993, Ed. F.A. Harris *et al.*, World Scientific, vol. I, p. 295; J.F. Gunion, *ibid.* p. 166.
- [10] I.F. Ginzburg, G.L. Kotkin, V.G. Serbo and V.I. Telnov, *Pis'ma ZhETF* 34 (1981) 514; *Nucl. Instr. Methods* 205 (1983) 47;
I.F. Ginzburg, G.L. Kotkin, S.L. Panfil, V.G. Serbo and V.I. Telnov, *Nucl. Instr. Methods* 219 (1984) 5.
- [11] O.J.P. Éboli, M.C. Gonzalez-Garcia, F. Halzen, and D. Zeppenfeld, *Phys. Rev.* **D48** (1993) 1440.

- [12] M. Baillargeon, G. Belanger and F. Boudjema, *Phys. Rev.* **D51** (1995) 4712.
- [13] B. Grzadkowski and J.F. Gunion, *Phys. Lett.* **B294** (1992) 361.
- [14] M. Kramer, J. Kühn, M.L. Stong, and P.M. Zerwas, *Z. Phys.* **C64** (1994) 21.
- [15] J.F. Gunion and H.E. Haber, *Nucl. Phys.* **B272** (1986) 1; *Nucl. Phys.* **B278** (1986) 449.
- [16] J.H. Kühn, E. Mirkes, J. Steegborn, *Z. Phys.* **C57** (1993) 615.
- [17] M. Drees, M. Krämer, J. Zunft and P.M. Zerwas, *Phys. Lett.* **B306** (1993) 371.
- [18] G. Jikia and A. Tkabladze, Proc. of the *Workshop on gamma-gamma colliders*, March 28-31, 1994, Lawrence Berkeley Laboratory, Nucl. Instr. and Meth. **A355**, 81-83, 1995.
- [19] B. Kamal, Z. Merebashvili and A.P. Contogouris, *Phys. Rev.* **D51** (1995) 4808.
- [20] J.F. Gunion and H.E. Haber, *Phys. Rev.* **D48** (1993) 5109.
- [21] G.J. van Oldenborgh and J.A.M. Vermaseren, *Z. Phys.* **C46** (1990) 425.
- [22] J.A.M. Vermaseren, Symbolic Manipulation with FORM, published by CAN, Kruislaan 413, 1098 SJ Amsterdam, 1991, ISBN 90-74116-01-9.
- [23] E.E. Boos et al., in the Proceedings of the XXVIth Rencontre de Moriond, ed. by J. Tran Than Van, Edition Frontiers, p.501 (1991);
E.E. Boos et al., in the Proceedings of the Second International Workshop on Software Engineering, ed. by D. Perret-Gallix, World Scientific, p.665 (1992);
V.A. Ilyin, D.N. Kovalenko and A.E. Pukhov, INP MSU Preprint-95-2/366, Moscow State University, (1995).
- [24] V.I. Telnov, Proceedings of the Workshop on Gamma-Gamma Colliders, LBL, March 28-31, 1994, Nucl. Instrum. Methods, **A355** (1995) 3.
- [25] E. Braaten and J.P. Leveille, *Phys. Rev.* **D22** (1980) 715;
M. Drees and K.-I. Hikasa, *Phys. Lett.* **B240** (1990) 455, *Phys. Rev.* **D41** (1990) 1547.
- [26] I.F. Ginzburg and V.G. Serbo, in Physics and Experiments with Linear e^+e^- Colliders, Waikoloa, Hawaii, 1993, Ed. F.A. Harris *et al.*, World Scientific, vol. II, p. 563.
- [27] G.P. Lepage, *J. Comput. Phys.* **27** (1978), 192.
- [28] J. Fujimoto, M. Igarashi, N. Nakazawa, Y. Shimizu and K. Tobimatsu, *Prog. Theor. Phys. Suppl.* No. 100 (1990) 1.

- [29] T. Kinoshita, *J. Math. Phys.* **3** (1962) 650;
T.D. Lee and M. Nauenberg, *Phys. Rev.* **133B** (1964) 1549.

Figures

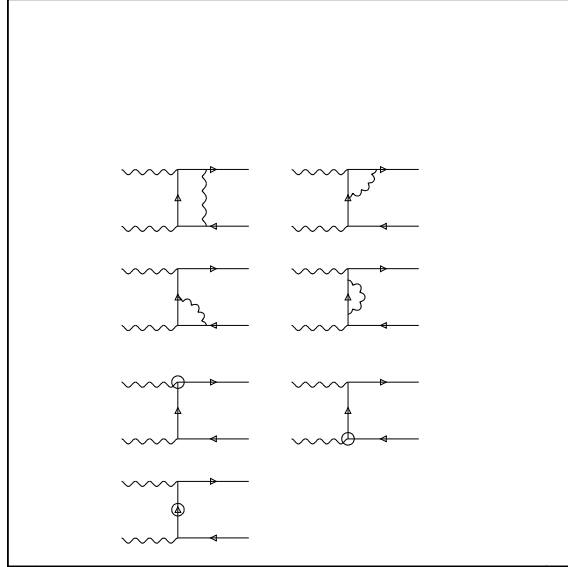


Fig. 1. Diagrams for QCD $\mathcal{O}(\alpha^2 \alpha_s)$ -corrections to the heavy quark production in $\gamma\gamma$ collisions.

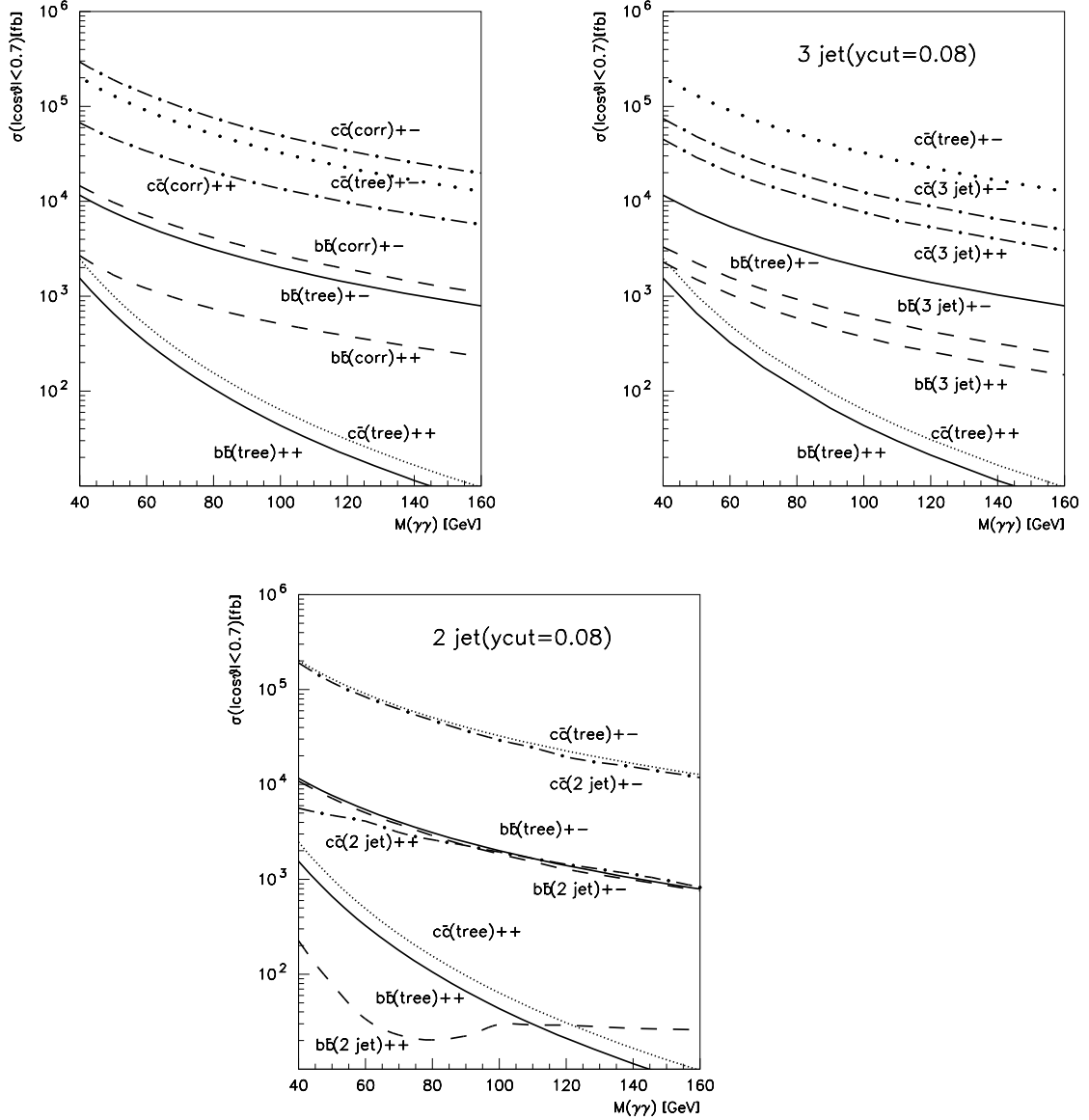


Fig. 2. $b\bar{b}/c\bar{c}$ -pair production cross sections in $\gamma\gamma$ collisions for various helicity states of colliding photons. Solid lines correspond to $\gamma\gamma \rightarrow b\bar{b}$ cross sections at tree level, dashed lines – to the radiatively corrected $b\bar{b}$ production cross sections; dotted lines – to $\gamma\gamma \rightarrow c\bar{c}$ cross sections at tree level and dash-dotted lines – to the corrected $c\bar{c}$ -pair productions; (a) total cross sections (i.e. two-jet plus three-jet), (b) and (c) three- and two-jet cross sections, respectively, with $y_{\text{cut}}=0.08$.

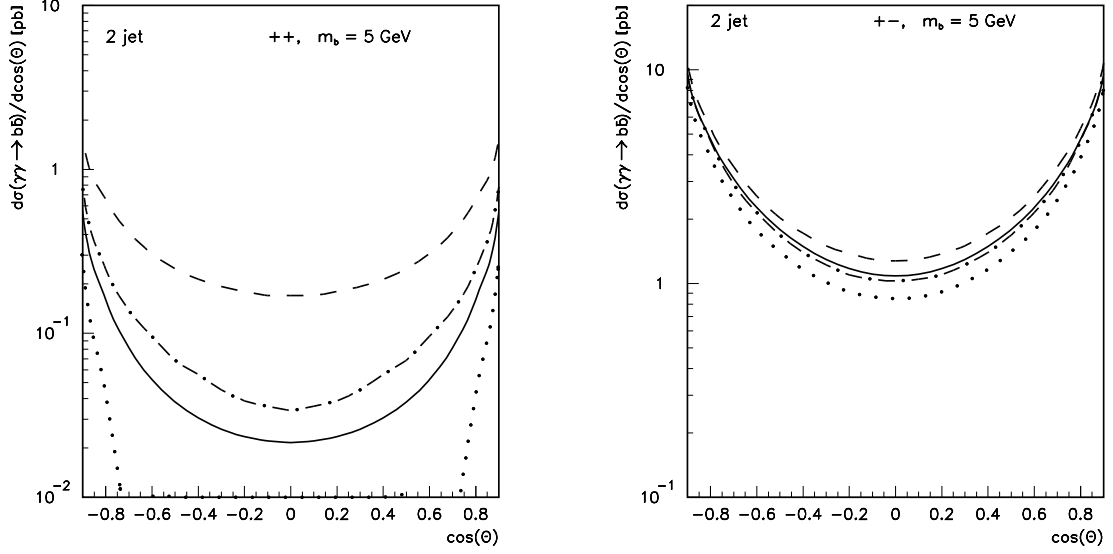


Fig. 3. Differential cross sections of the $b\bar{b}$ -pair production versus b-quark scattering angle at $\sqrt{s} = 100$ GeV. Solid line corresponds to tree level cross section, dashed line – total cross section, dash-dotted line – two-jet cross section with $y_{cut} = 0.08$ and dotted line – two-jet cross section with $y_{cut} = 0.04$; (a) cross sections for $J_z = 0$ and (b) for $J_z = \pm 2$.

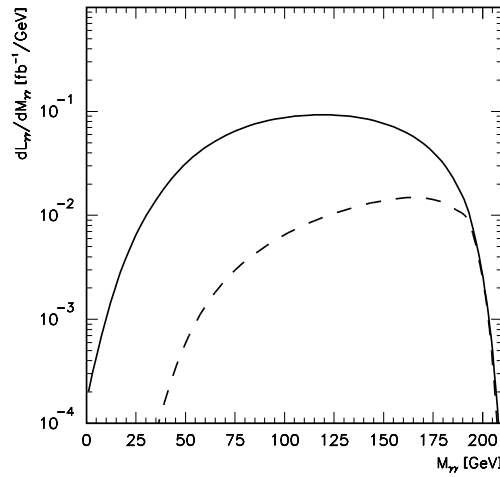


Fig. 4. The spread $\gamma\gamma$ luminosity distributions to be used in a search for intermediate-mass Higgs boson. The integrated e^+e^- luminosity of 20 fb^{-1} is assumed.

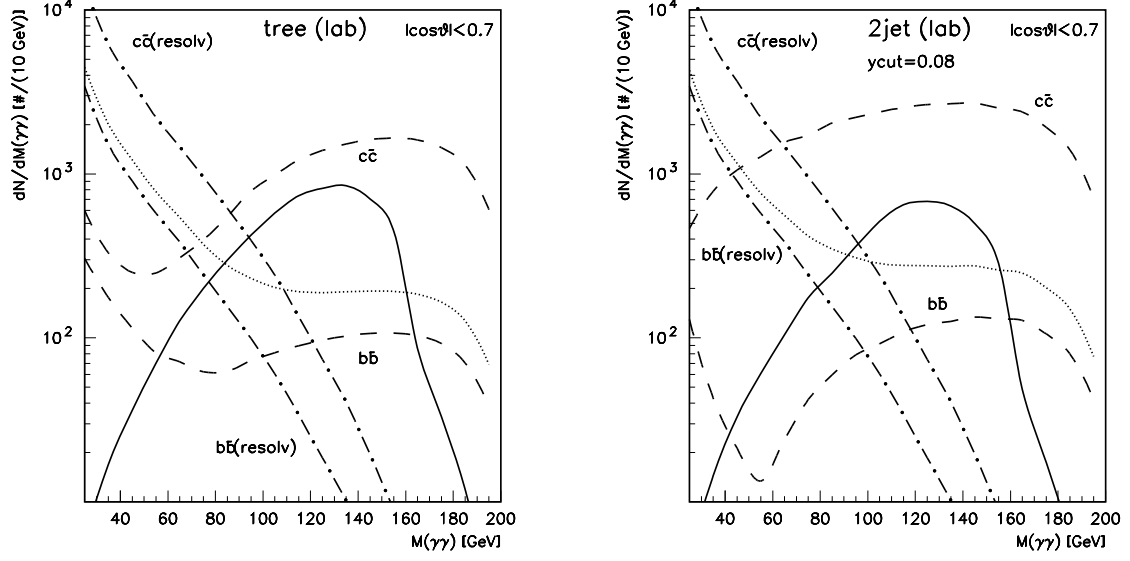


Fig. 5. Expected event rates for search for an intermediate-mass Higgs boson in two jet events. Solid lines correspond to signal events, dashed lines – to background events ($\gamma\gamma \rightarrow c\bar{c}$ and $\gamma\gamma \rightarrow b\bar{b}$), dash-dotted lines – to resolved photon contributions ($\gamma\gamma \rightarrow b\bar{b}(c\bar{c})$); (a) tree level results and (b) signal and backgrounds with QCD corrections. Dotted line in Figure (b) corresponds to the total background ($b\bar{b} + c\bar{c}$).

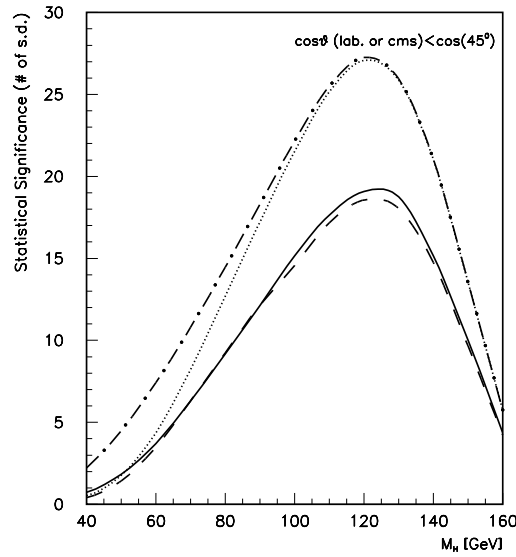


Fig. 6. Statistical significance of the Higgs boson signal corresponding to the event rates in Fig. 5. Solid line corresponds to the event rates with QCD corrections (angular cut in the lab. system), dashed line – to the same ones with angular cut in the c.m.s., dash-dotted line – to the tree level rates without resolved photon contribution [6], and dotted line – to tree level rates with account of resolved photon contribution.

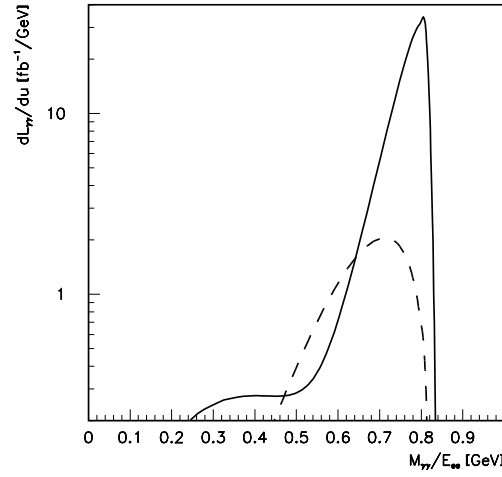


Fig. 7. The peaked $\gamma\gamma$ luminosity distribution to be used for a precise measurement of the two-photon width of a Higgs boson.

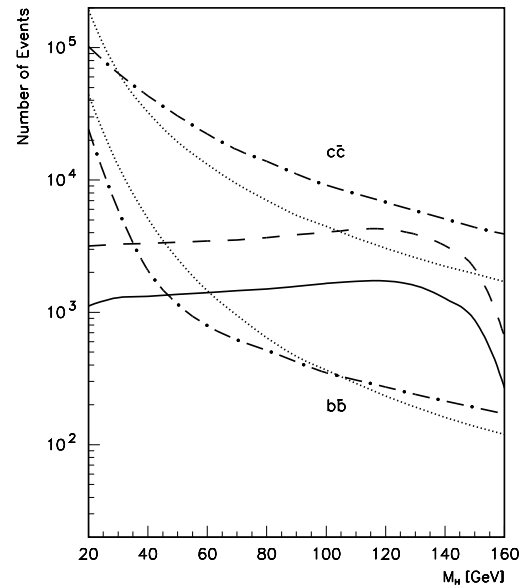


Fig. 8. Expected number of the signal and the background events for an experiment designed to measure the two-photon width of Higgs boson. Solid line corresponds to signal events with QCD corrections, dashed line – to signal events at tree level, dash-dotted lines – to background events with QCD corrections and dotted line – to background events at tree level.

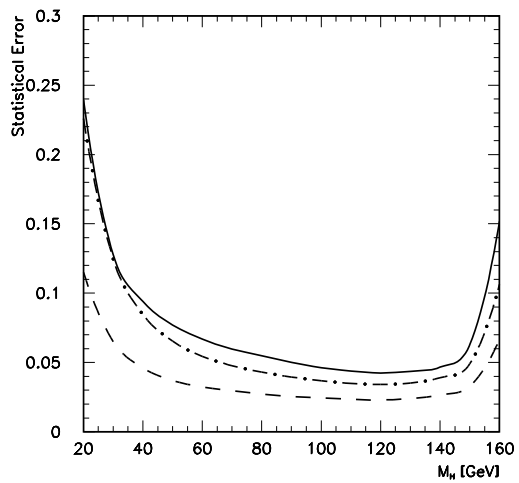


Fig. 9. The statistical error in the measurement of the $\Gamma(H \rightarrow \gamma\gamma)$ for the event rates given in Fig. 8. Dashed line corresponds to tree level rates with angular cut in the lab. system, solid line – to event rates with QCD corrections and dash-dotted line – to tree level results from [6] (angular cut in the c.m.s.).